Photonics-Aided Millimeter-Wave Technologies for Extreme Mobile Broadband Communications in 5G

Xinying Li, *Member, IEEE, Member, OSA*, Jianjun Yu, *Senior Member, IEEE, Fellow, OSA*, and Gee-Kung Chang, *Fellow, IEEE, Fellow, OSA*

(Invited Paper)

***Abstract*—To meet the enhanced-mobile-broadband (eMBB) challenges in 5G, we have systematically explored the potential of the photonics-aided millimeter-wave (mm-wave) communication in terms of the wireless transmission capacity and distance it can accommodate. Enabled by various kinds of advanced multiplexing and digital-signal-processing (DSP) techniques, we have successfully achieved the significant enhancement of the wireless mm-wave signal transmission capacity from 100 Gb/s to 400 Gb/s, even to 1 Tb/s. Since our large-capacity (>100-Gb/s) experimental demonstrations typically have a very short wireless transmission distance of several meters, we have further explored the techniques for the extension of the wireless mm-wave signal transmission distance, and successfully achieved a series of field-trial demonstrations on photonics-aided long-distance (>100-m) wireless mm-wave signal transmission. We have realized the record-breaking product of wireless transmission capacity and distance, i.e., 54 Gb/s × 2.5 km.**

***Index Terms*—Enhanced mobile broadband (eMBB), large-capacity wireless transmission, long-distance wireless transmission, millimeter-wave communication, multiplexing, digital signal processing, photonics-aided technology.**

I. Introduction

IT IS well known that the fiber-optic communication can provide huge transmission capacity and ultra-long transmission distance. But it has no mobility, and cannot realize wide-area seamless coverage. The millimeter-wave (mm-wave) wireless communication can cover anywhere in theory. But it has limited available spectrum resources, and it can also easily affected by various impairments. Therefore, the mm-wave wireless communication has very limited transmission distance. The mm-wave fiber-wireless-integration (FWI) communication combines the advantages of both fiber-optic communication and mm-wave wireless communication, and can meet the requirements of future communication networks for both communication bandwidth and mobility [1]–[9]. Therefore, the mm-wave FWI communication has various kinds of application scenarios, such as 5G and beyond mobile communication, indoor broadband network, defense space communication, large-capacity emergency communication, and so on.

There are several typical techniques which can be used to realize large-capacity fiber-optic transmission, including optical polarization multiplexing, high-level quadrature-amplitude-modulation (QAM) modulation, electrical/optical multi-carrier modulation, as well as advanced transmitter-based and receiver-based digital-signal-processing (DSP) algorithms. Particularly, the advanced DSP algorithms can be used to compensate for various linear and nonlinear impairments from components and fiber-optic transmission links, and therefore will improve the receiver sensitivity and system performance [10]–[15]. In order to make the mm-wave wireless transmission to match the large-capacity fiber-optic transmission, we can introduce the aforementioned optical communication techniques into the wireless mm-wave systems [16]–[29]. In this case, we need to investigate how to realize the generation and wireless transmission of the polarization-multiplexing mm-wave signal, the high-level QAM modulated mm-wave signal, as well as the multi-carrier mm-wave signal, based on the photonics-aided technology. We also need to investigate the realization and integration of various kinds of advanced techniques within the mm-wave band to realize large-capacity wireless mm-wave signal transmission. The introduction of the aforementioned optical communication techniques into the wireless mm-wave systems can reduce the transmission baud rate, increase the transmission capacity, and promote the seamless integration of fiber-optic communication and mm-wave wireless communication systems [6]–[9]. In the meantime, the advanced coherent DSP algorithms will also be required by the wireless mm-wave systems to recover the multi-dimensional multi-level mm-wave signal and to enhance system performance [6]–[9].

Manuscript received May 24, 2019; revised August 5, 2019; accepted August 9, 2019. Date of publication August 13, 2019; date of current version January 23, 2020. This work was supported by the National Key Research and Development Program of China under Grant 2018YFB1801703 and in part by the National Natural Science Foundation of China under Grants 61527801, 61675048, 61720106015, 61835002, 61805043, 61922025, and 61935005. This paper was presented in part at the Optical Fiber Communication Conference and Exhibition, San Diego, CA, USA, March 2019. *(Corresponding author: Xinying Li.)*

X. Li is with the Shanghai Institute for Advanced Communication and Data Science, Key Laboratory for Information Science of Electromagnetic Waves (MoE), State Key Laboratory of ASIC and System, Fudan University, Shanghai 200433, China, and also with the Georgia Institute of Technology, Atlanta, GA 30332 USA (e-mail: smileseaxy@gmail.com).

J. Yu is with the Shanghai Institute for Advanced Communication and Data Science, Key Laboratory for Information Science of Electromagnetic Waves (MoE), Fudan University, Shanghai 200433, China (e-mail: jianjun@fudan.edu.cn).

G.-K. Chang is with the Georgia Institute of Technology, Atlanta, GA 30332 USA (e-mail: geekung.chang@ece.gatech.edu).

Color versions of one or more of the figures in this paper are available online at http://ieeexplore.ieee.org.

Digital Object Identifier 10.1109/JLT.2019.2935137

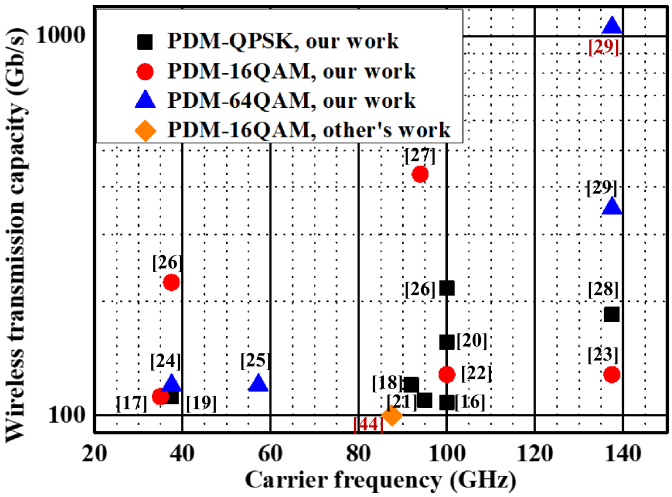

Fig. 1. Our experimental demonstrations on photonics-aided large-capacity (>100-Gb/s) wireless mm-wave signal transmission.

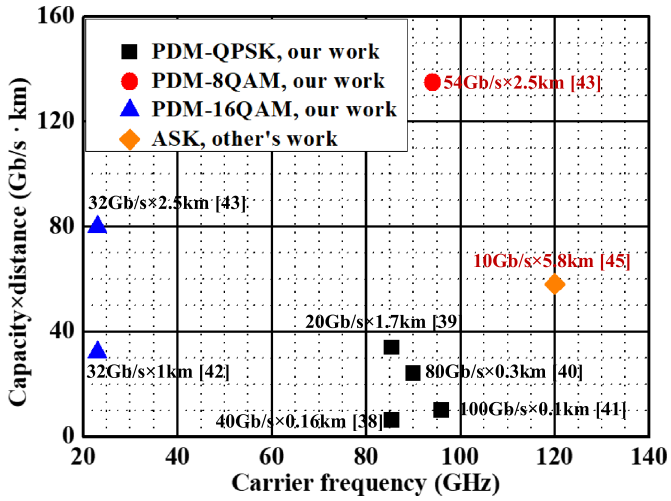

Fig. 2. Our experimental demonstrations on photonics-aided long-distance (>100-m) wireless mm-wave signal transmission.

Here, we would like to emphasize that, the enhanced mobile broadband (eMBB) communications, as one of the three typical application scenarios of the 5G mobile communication networks, will be required to meet the demands of future ubiquitous virtual reality/augmented reality (VR/AR), 4k/8k high-definition video, artificial intelligence, and so on. Therefore, eMBB will motivate the explosive increase of mobile data traffic and rates, which requires more bandwidth at higher carrier frequencies. Mm-wave band (30 GHz–300 GHz) is one of the promising candidates for 5G, since it has larger available bandwidth to accommodate higher mobile data traffic and rates [30]–[37]. Therefore, it is interesting to explore the potential of the mm-wave band in terms of the mobile data capacity it can accommodate, and to investigate how to realize mobile data transmission within the mm-wave band at a data rate as high as possible.

In the past several years, based on the photonics-aided technology, we have systematically explored the potential of various mm-wave bands, particularly the Q-band (33 GHz–50 GHz), the V-band (50 GHz–75 GHz), the W-band (75 GHz–110 GHz), and the D-band (110 GHz–170 GHz) [16]–[29], [38]–[43]. We have investigated the largest wireless transmission capacity they can accommodate [16]–[29] as well as the longest wireless transmission distance they can provide [38]–[43]. Fig. 1 summaries our demonstrated >100-Gb/s photonics-aided large-capacity wireless mm-wave signal transmission in terms of the employed mm-wave carrier frequencies, the employed high-order vector modulation, and the achieved wireless transmission capacity. We can see from Fig. 1 that our >100-Gb/s experimental demonstrations are mainly located at 40-GHz Q-band, 60-GHz V-band, 100-GHz W-band, and 140-GHz D-band. The mainly employed high-order vector modulation is polarization-division-multiplexing quadrature-phase-shift-keying (PDM-QPSK), polarization-division-multiplexing 16-ary quadrature-amplitude-modulation (PDM-16QAM), and PDM-64QAM. With our continuous efforts and exploration, we have successfully achieved the significant enhancement of the wireless transmission capacity from 100 Gb/s to 400 Gb/s, even to 1Tb/s. We can also see from Fig. 1 that, the higher mm-wave carrier frequencies, for example, the 100-GHz W-band and 140-GHz D-band, and the higher-order vector modulation, such as 16QAM and 64QAM, are more suitable for the realization of larger wireless transmission capacity. Our record-breaking 432-Gb/s wireless transmission capacity is enabled by 100-GHz W-band and 16QAM modulation [27], while our record-breaking 1.056-Tb/s wireless transmission capacity is enabled by 140-GHz D-band and 64QAM modulation [29]. As a comparison, we also listed in Fig. 1 the most representative large-capacity achievement from other research groups. That is, in 2011, X. Pang et al. demonstrated a photonics-aided PDM-16QAM mm-wave signal transmission at 87.5-GHz W-band carrier frequency with a wireless transmission capacity of 100 Gb/s, which is evidently lower than our achievements [44].

We also have successfully achieved a series of field-trial demonstrations on photonics-aided long-distance (>100-m) wireless mm-wave signal transmission, as shown in Fig. 2. All our field-trial demonstrations are carried out under a good weather and line-of-sight (LOS) transmission. We can see from Fig. 2 that our field-trial demonstrations are mainly located at 20-GHz K-band (18 GHz–27 GHz) and 90-GHz W-band, since these two bands have relatively low atmospheric loss. The mainly employed vector modulation is relatively low-order QPSK, 8QAM, and 16QAM. The largest product of wireless transmission capacity and distance, i.e., 54 Gb/s × 2.5 km = 135 Gb/s·km, has been achieved at 90-GHz W-band with 8QAM modulation [43]. Similarly, as a comparison, we also listed in Fig. 2 the most representative long-distance achievement from other research groups. That is, in 2012, A. Hirata et al. demonstrated a photonics-aided 10-Gb/s mm-wave signal transmission at 120-GHz D-band carrier frequency with a wireless transmission distance of 5.8 km [45]. The corresponding product of wireless transmission capacity and distance, i.e., 58 Gb/s·km, is evidently smaller than our largest achievement of 135 Gb/s·km.

The remainder of the paper is just as follows. Section II will introduce various multiplexing and DSP techniques which we have used to realize >100-Gb/s photonics-aided large-capacity wireless mm-wave signal transmission, as well as corresponding experimental demonstrations. Since our large-capacity (>100-Gb/s) experimental demonstrations typically have a very short wireless transmission distance of several meters, we have further explored the techniques for the extension of the wireless mm-wave signal transmission distance and successfully achieved a series of field-trial demonstrations on >100-m photonics-aided long-distance wireless mm-wave signal transmission, which will be introduced in detail in Section III. Section IV gives our conclusions.

II. Multiplexing and DSP Techniques for >100-Gb/s Large-Capacity Wireless Transmission

In this Section, we will mainly introduce seven kinds of multiplexing and DSP techniques which we have used to realize >100-Gb/s large-capacity wireless mm-wave signal transmission. These techniques include photonics-aided mm-wave generation, heterodyne coherent detection combined with advanced DSP, wireless multiple-input multiple-output (MIMO) with optical polarization multiplexing, optical multi-carrier modulation, antenna polarization multiplexing, multiple mm-wave frequency multiplexing, and probabilistic constellation shaping (PS). The introduction of these techniques into the photonics-aided mm-wave signal communication systems can typically reduce the signal transmission baud rate and loosen the bandwidth requirement for optical and electrical devices, and therefore enhance the wireless transmission capacity.

A. Photonics-Aided Mm-Wave Generation

The methods for the mm-wave signal generation include electrical ones and photonics-aided ones. The methods for the electrical mm-wave signal generation typically have a simple structure and are easy for system integration. However, the commercially available electrical devices usually have very limited bandwidth, and meantime the manufacture of higher-frequency radio-frequency (RF) devices is relatively difficult and expensive [46]–[51]. As a result, it is very difficult, and even impractical, to generate the wideband and high-carrier-frequency mm-wave signal, only based on electrical devices.

Photonics-aided mm-wave signal generation can overcome the bandwidth limitation of electrical devices, and is more suitable for the generation of the wideband and high-carrier-frequency mm-wave signal [52]–[55]. Fig. 3 gives the basic principle of photonics-aided mm-wave signal generation. The generation of two optical carriers spaced by a certain frequency f_s as well as their heterodyne beating in a high-speed photodetector (PD) are key for photonics-aided mm-wave signal generation. Here, the optical carrier at frequency of $(f_c + f_s)$ is used to carry the transmitter data, while the optical carrier at frequency of f_c functions as the optical local oscillator (LO). Their frequency spacing f_s is just located within the mm-wave band. After optical coupling, we can get an optical mm-wave signal at carrier frequency of f_s. We then use a high-speed PD

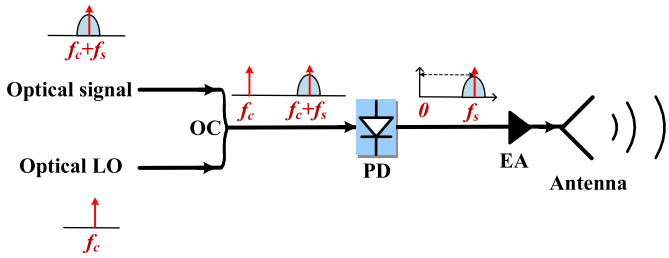

Fig. 3. The basic principle of photonics-aided mm-wave signal generation. LO: local oscillator, OC: optical coupler, PD: photodetector, EA: electrical amplifier.

to realize the optical-to-electrical conversion to get the electrical mm-wave signal at carrier frequency of f_s.

As for the generation of the aforementioned two optical carriers, the methods in the early days are mainly based on a kind of structure of a single laser source cascaded with external optical modulation [7], [9]. This kind of structure can generate two or more optical subcarriers enabled by the nonlinear effect of the optical modulator, and an additional optical filter is required when the number of the generated optical subcarriers is over two, in order to select the two desired optical subcarriers. Based on this kind of structure, we can use low-frequency RF driving signal to generate high-carrier-frequency mm-wave signal via photonic frequency multiplication, which significantly reduces the bandwidth requirement for electrical and optical components at the transmitter end. However, the optical power from the single laser source is shared by multiple optical subcarriers, and therefore the generated mm-wave signal has a relatively low signal-to-noise ratio (SNR). Moreover, the generated high-frequency mm-wave carrier by this kind of structure will occupy most of the available bandwidth of the optical modulator, and therefore the signal it carries cannot have very large bandwidth.

Very recently, two free-running laser sources have been mainly used to generate the aforementioned two optical carriers, in order to realize the ultra-wideband mm-wave signal generation [16]–[29]. This kind of structure can be used to generate the mm-wave signal with high SNR, which is capable of carrying the ultra-high-speed transmitter data. However, the free-running characteristic of the two laser sources will lead to the drift of both carrier frequency and phase, which is needed to eliminate at the receiver end, particularly for the vector mm-wave signal generation. Luckily, this problem has been perfectly resolved by fast-developing coherent detection techniques and advanced DSP algorithms, particularly the receiver- and DSP-based carrier recovery algorithms.

B. Heterodyne Coherent Detection Combined With Advanced DSP

As mentioned in the introduction, the application of advanced optical communication techniques, including optical polarization multiplexing, high-level QAM modulation, electrical/optical multi-carrier modulation and so on, into the wireless mm-wave systems, can reduce the transmission baud rate, increase the transmission capacity, and make the mm-wave

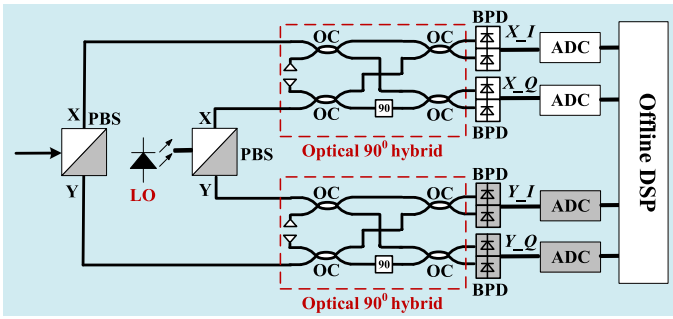

Fig. 4. The integrated structure for heterodyne coherent detection combined with DSP. PBS: polarization beam splitter, LO: local oscillator, OC: optical coupler, BPD: balanced photodetector, ADC: analog-to-digital converter.

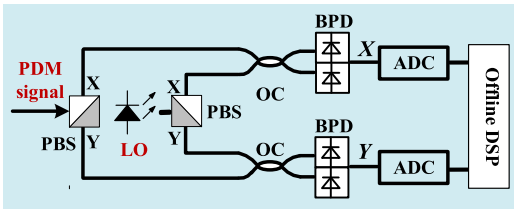

Fig. 5. The simplified structure for heterodyne coherent detection combined with DSP. PBS: polarization beam splitter, LO: local oscillator, OC: optical coupler, BPD: balanced photodetector, ADC: analog-to-digital converter.

wireless transmission to better match large-capacity fiber-optic transmission. In this scenario, heterodyne coherent detection, combined with advanced DSP algorithms, is required to detect the multi-dimensional multi-level mm-wave signal and to enhance the system performance [16]–[29].

Figs. 4 and 5 gives the integrated and simplified structures for heterodyne coherent detection combined with advanced DSP, respectively. We can see from Fig. 4 that, the integrated structure for heterodyne coherent detection includes two polarization beam splitters (PBSs), two optical 90° hybrids, and four balanced photodiodes (BPDs). Two PBSs and two optical 90° hybrids are used to implement the polarization diversity and phase diversity of the polarization-multiplexing optical signal and optical LO in the optical domain, and typically, they are monolithically integrated in the commercially available products. Since optical phase diversity is unnecessary for heterodyne coherent detection, the monolithically integrated two PBSs and two optical 90° hybrids can be simplified into two PBSs and two optical couplers (OC), just as shown in Fig. 5. The number of the required BPDs and ADCs can be also reduced by half, since the in-phase (I) and quadrature (Q) signal components at each polarization (X- or Y-polarization) are still combined together and there are simply two different signal tributaries after optical polarization diversity. Obviously, the simplified structure for heterodyne coherent detection is more hardware efficient than its corresponding integrated structure. Moreover, thanks to the availability of high-speed large-bandwidth BPDs and analog-to-digital converters (ADCs), the intermediate-frequency (IF) down conversion as well as the separation of I and Q signal components can be realized in the digital domain via offline DSP [16].

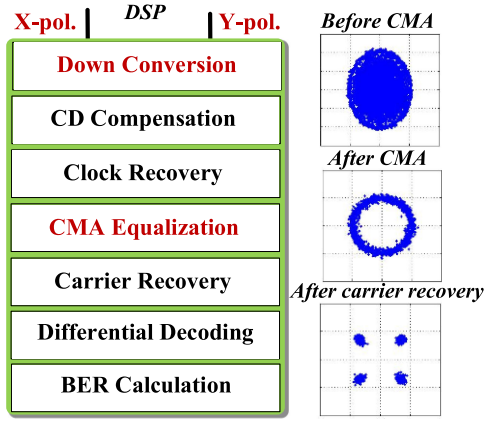

Fig. 6. Receiver-based offline DSP for PDM-QPSK signal as well as recovered constellations before CMA equalization, after CMA equalization, and after carrier recovery, respectively.

Particularly, for optical PDM-QPSK modulation, the detailed offline DSP after heterodyne coherent detection includes IF down conversion, chromatic dispersion (CD) compensation, clock recovery, constant-modulus-algorithm (CMA) equalization, carrier recovery, differential decoding, and bit-error-ratio (BER) calculation [16], just as shown in Fig. 6. Here, the CMA equalization is used to realize the signal polarization de-multiplexing for the PDM-QPSK signal. The three inserted recovered constellations in Fig. 6 correspond to the DSP procedures before CMA equalization, after CMA equalization, and after carrier recovery, respectively. For optical PDM-16QAM modulation, during the offline DSP, we use the cascaded multi-modulus algorithm (CMMA) equalization, instead of CMA equalization, to realize signal polarization de-multiplexing for the three-modulus PDM-16QAM signal [17]. For optical PDM-64QAM modulation, during the offline DSP, we need to add large-tap T-spaced decision-directed least-mean-square (DD-LMS) equalization after carrier recovery [24], [25]. Compared to QPSK and 16QAM, 64QAM has a shorter Euclidean distance and worse tolerance to noise. The large-tap T-spaced DD-LMS equalization, based on stochastic gradient descent method, can eliminate the phase noise and converge each constellation points. Therefore, its employment can significantly improve the system performance with the PDM-64QAM modulation.

It is worth noting that, in our experimental demonstrations on photonics-aided large-capacity (>100-Gb/s) wireless mm-wave signal transmission, we typically employ the simplified structure of heterodyne coherent detection as shown in Fig. 5 for PDM-QPSK and PDM-16QAM modulation [16]–[23], [26], [27], while we employ the integrated structure of heterodyne coherent detection as shown in Fig. 4 for PDM-64QAM modulation [24], [25], [29]. This is because PDM-64QAM modulation has a higher requirement for the system stability than PDM-QPSK and PDM-16QAM modulation, while the integrated version with monolithically integrated PBSs and optical 90° hybrids is more stable than the simplified version with separate PBSs and OCs. In addition, when we use the integrated version to detect the PDM-64QAM signal, we simply use two output ports of each

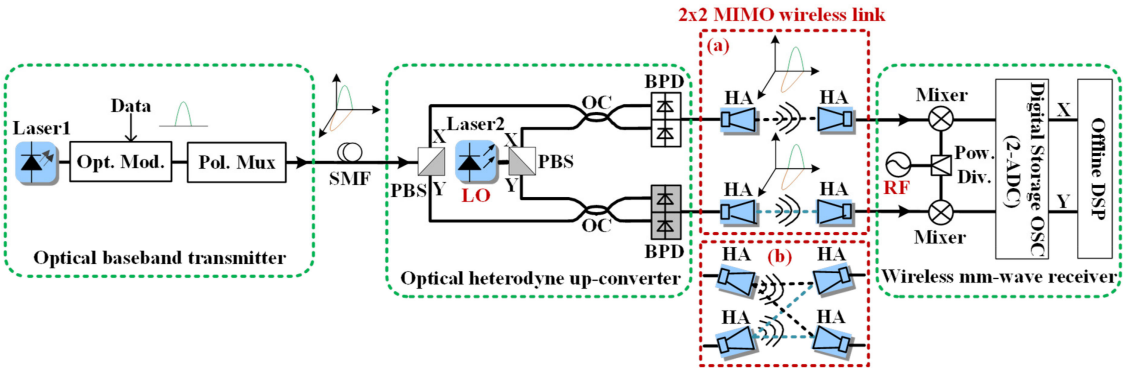

Fig. 7. Principle and schematic diagram for the technique of wireless MIMO with optical polarization multiplexing to realize the generation and wireless transmission of the polarization-multiplexing mm-wave signal. Opt. Mod.: optical modulator, Pol. Mux: polarization multiplexer, SMF: single-mode fiber, PBS: polarization beam splitter, LO: local oscillator, OC: optical coupler, BPD: balanced photodiode, HA: horn antenna, RF: radio frequency, Pow. Div.: power divider, OSC: oscilloscope, ADC: analog-to-digital converter, DSP: digital signal processing.

Wireless capacity	Wireless distance	Mm-wave band	Carrier frequency	Modulation format	BER threshold	Applied techniques and Refs.
108Gb/s	1m	W-band	100GHz	PDM-QPSK	3.8×10^{-3}	T-I [16, 67]
109.6Gb/s	2m	W-band	95GHz	PDM-QPSK	2×10^{-2}	T-I [68]
144Gb/s	2m	W-band	100GHz	PDM-QPSK	3.8×10^{-3}	T-I [20, 69]
184Gb/s	0.6m	D-band	137.5GHz	PDM-QPSK	2×10^{-2}	T-I [23]
112Gb/s	0.5m	Q-band	35GHz	PDM-16QAM	3.8×10^{-3}	T-I [17]
128Gb/s	1m	W-band	100GHz	PDM-16QAM	2×10^{-2}	T-I [22]
128Gb/s	0.1m	D-band	137.5GHz	PDM-16QAM	2×10^{-2}	T-I [23]
120Gb/s	1m	Q-band	37.5GHz	PDM-64QAM	3.8×10^{-3}	T-I [24]
120Gb/s	1m	V-band	57.2GHz	PDM-64QAM	3.8×10^{-3}	T-I [25]

Fig. 8. Our 100 Gb/s-class experimental demonstrations based on T-I. T-I: wireless MIMO with optical polarization multiplexing.

optical 90° hybrid, and therefore only two BPDs and two ADCs are required in this scenario.

C. Wireless MIMO With Optical Polarization Multiplexing

On the one hand, it is well known that the technique of optical polarization multiplexing can be used to double the capacity of a fiber-optic link, and it is a practical solution for the future spectrally-efficient high-speed optical transmission. Therefore, it is interesting to investigate how to realize the generation and wireless transmission of the polarization-multiplexing mm-wave signal, in order to realize the FWI communication. After polarization multiplexing, the mm-wave signal can be converted from two-dimension to three-dimension, and therefore the wireless transmission capacity can be doubled. On the other hand, we can use a single-input single-output (SISO) wireless link to deliver the single-polarization mm-wave signal [56]–[60]. For the delivery of the polarization-multiplexing mm-wave signal, however, we need to use a 2×2 MIMO wireless link based on two pairs of antennas [61]–[67].

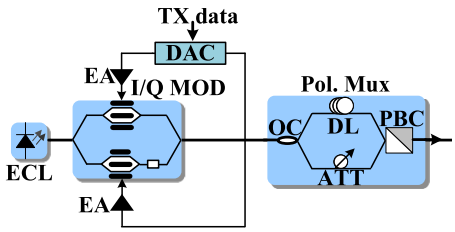

Fig. 9. The detailed structure of the optical baseband transmitter in our experimental demonstrations for optical PDM-QPSK/PDM-16QAM/PDM-64QAM modulation. ECL: external cavity laser, EA: electrical amplifier, I/Q MOD: I/Q modulator, DAC: digital-to-analog converter, Pol. Mux: polarization multiplexer, OC: optical coupler, DL: optical delay line, ATT: optical attenuator, PBC: polarization beam combiner.

In this case, we have proposed the technique of wireless MIMO with optical polarization multiplexing to realize the generation and wireless transmission of the polarization-multiplexing mm-wave signal [16], [67]. In the following part, we will use T-I to denote this technique for simplification. Fig. 7

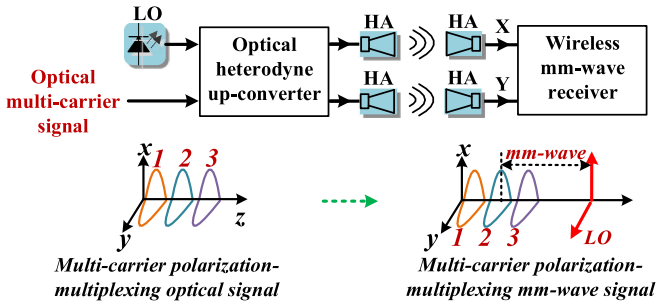

Fig. 10. Principle and schematic diagram for the photonics-aided mm-wave system based on the integration of TI and T-II to realize the generation and wireless transmission of the multi-carrier polarization-multiplexing mm-wave signal. LO: local oscillator, HA: horn antenna.

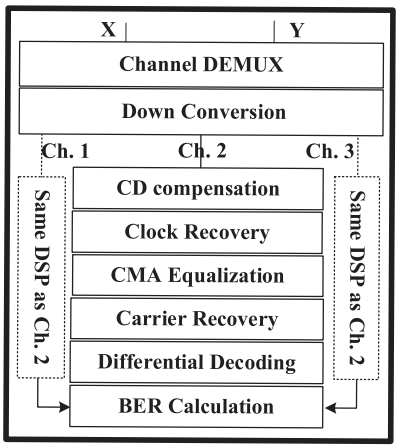

Fig. 11. Receiver-based joint-channel DSP for multi-carrier polarization-multiplexing mm-wave signal.

gives the principle of T-I. The overall system structure includes five parts, i.e., the optical baseband transmitter, the fiber link, the optical heterodyne up-converter, the 2 × 2 MIMO wireless link, and the wireless mm-wave receiver.

At the optical baseband transmitter, we use an optical modulator and a polarization multiplexer to generate the polarization-multiplexing optical baseband signal. After fiber transmission, the polarization-multiplexing optical baseband signal is received by the optical heterodyne up-converter. At the optical heterodyne up-converter, we use two PBSs and two OCs to perform the operation of optical polarization diversity for the received optical baseband signal and the LO signal. The optical LO signal is generated from Laser 2. Here, it is worth noting that, both Laser 2 at the optical up-converter and Laser 1 at the optical transmitter are free-running, and their frequency spacing is just our desired mm-wave carrier frequency. It is also worth noting that, in our corresponding experimental system [67], both Laser 1 and Laser 2 are typically commercially available external cavity lasers (ECLs) with a laser linewidth less than 100 kHz, and their operating frequency is around 193.1 THz. Therefore, we can calculate the frequency deviation of our experimental systems is about 0.001 ppm, which is quite small. Moreover, the frequency deviation caused by the laser linewidth can be effectively eliminated by our DSP-based carrier recovery algorithms at the receiver end. Then, we use two parallel PDs to perform the optical-to-electrical conversion to generate two electrical mm-wave signals, which can be considered as a polarization-multiplexing electrical mm-wave signal. The two PDs can be single-ended ones or balanced ones. Compared to the single-ended PD, the BPD can eliminate the noise and increase the system stability. Here, it is worth noting that each output of the PBS with the input of the optical baseband signal contains both X- and Y-polarization transmitter data encoded at the optical baseband transmitter, because of the polarization rotation caused by fiber transmission, and we use the labeling of 'X' and 'Y' in Fig. 7 for simplification.

We then use the 2 × 2 MIMO wireless link to deliver the generated polarization-multiplexing electrical mm-wave signal. In some cases, each receiver antenna can simultaneously receive the wireless power from two transmitter antennas, and therefore wireless crosstalk may occur. At the wireless mm-wave receiver, we first use the analog down conversion based on balanced mixer and sinusoidal RF signal, to down-convert the high-frequency mm-wave signal to a lower-frequency IF signal. We then use a dual-channel digital storage oscilloscope (OSC) to capture the IF signal for the subsequent offline DSP. For a polarization-multiplexing signal, both fiber link and 2 × 2 MIMO wireless link can be considered as a 2 × 2 model, and denoted by a 2 × 2 Jones matrix. Since the product of two 2 × 2 Jones matrixes is still a 2 × 2 matrix, we can use receiver-based CMA/CMMA algorithms to perform the signal polarization de-multiplexing and wireless crosstalk suppression at the same time [18].

Fig. 8 summarizes our 100 Gb/s-class experimental demonstrations based on T-I. For example, we have realized 108-Gb/s signal delivery over 1-m wireless distance at W-band [16], [67], 112-Gb/s signal delivery over 0.5-m wireless distance at Q-band [17], 120-Gb/s signal delivery over 1-m wireless distance at V-band [25], and so on. It is worth noting that our experimental demonstrations mainly employ PDM-QPSK, PDM-16QAM, and PDM-64QAM modulation.

Fig. 9 gives the detailed structure of the optical baseband transmitter in our aforementioned 100 Gb/s-class experimental demonstrations, which can realize optical PDM-QPSK/PDM-16QAM/PDM-64QAM modulation. The optical baseband transmitter mainly includes a free-running ECL, an in-phase/quadrature (I/Q) modulator, and a polarization multiplexer. The I/Q modulator is made up of two Mach-Zehnder intensity modulators (MZ-IMs) and a phase modulator. By adjusting the three DC-biases of the I/Q modulator, we can make the two MZ-IMs operate at the null point and the phase modulator operate at a $\pi/2$ phase shift. In the case, when we use an electrical binary/four-level/six-level signal to drive the I/Q modulator, we can realize optical QSPK/16QAM/64QAM modulation, respectively. The polarization multiplexer includes a polarization-maintaining OC to equally split the output of the I/Q modulator into two tributaries, an optical delay line in one arm to create 150-symbol delay for one tributary, an optical attenuator in the other arm to balance the optical power of two tributaries, and a polarization beam combiner (PBC) to recombine the two tributaries. After the polarization multiplexer, we

Wireless capacity	Wireless distance	Mm-wave band	Carrier frequency	Modulation format	BER threshold	Applied techniques and Refs.
120Gb/s	2m	W-band	92GHz	PDM-QPSK	3.8×10^{-3}	T-I, T-II [18]
120Gb/s	1.4m	THz-band	437.5GHz	PDM-QPSK	3.8×10^{-3}	T-I, T-II [73, 74]

Fig. 12. Our 100 Gb/s-class experimental demonstrations based on the integration of T-I and T-II. T-I: wireless MIMO with optical polarization multiplexing. T-II: optical multi-carrier modulation.

can get a PDM-QPSK/PDM-16QAM/PDM-64QAM modulated optical baseband signal. It is worth noting that, the higher the modulation order, the larger the bit number per symbol and the lower the required signal baud rate. But at the same time, a higher receiver sensitivity is also required with the increase of the modulation order. Therefore there is a tradeoff between the optimal vector modulation and the overall system performance [70]–[72].

D. Optical Multi-Carrier Modulation

We further introduce the second technique of the optical multi-carrier modulation, denoted by T-II, into our mm-wave systems to increase the wireless transmission capacity. The employment of T-II, such as optical orthogonal-frequency-division-multiplexing (OFDM) and Nyquist wavelength division multiplexing (WDM), gives the possibility for optical sub-carrier optimization [18], [62].

Fig. 10 gives the schematic diagram of the photonics-aided mm-wave system based on the integration of T-I and T-II, which can be used to realize the generation and wireless transmission of the multi-carrier polarization-multiplexing mm-wave signal [18]. Here, we take a three-channel WDM signal as an example. The mm-wave carrier frequency is the frequency spacing between Channel 2 and the optical LO signal. We have used the same optical heterodyne up-converter, 2 × 2 MIMO wireless link, and wireless mm-wave receiver as mentioned in Section IIA. At the wireless mm-wave receiver, after analog down conversion, we can get an IF signal with full-channel information. Therefore, we can use the receiver-based joint-channel DSP, as shown in Fig. 11, to deal with the IF signal and recover all the three WDM channels at the same time [18]. We can see from Fig. 11 that the channel de-multiplexing is implemented in the digital domain. After simultaneous down conversion to baseband, we individually implement the same DSP operation, from CD compensation to BER calculation, for all the three WDM channels. Fig. 12 summarizes our 100 Gb/s-class experimental demonstrations within both the W-band and Terahertz-band (THz-band), based on the integration of T-I and T-II.

E. Antenna Polarization Multiplexing

We further introduce the third technique of the antenna polarization multiplexing, denoted by T-III, into our mm-wave systems to increase the wireless transmission capacity. Fig. 13 gives the schematic diagram of the photonics-aided mm-wave system based on the integration of T-I, T-II, and T-III [19]. Here,

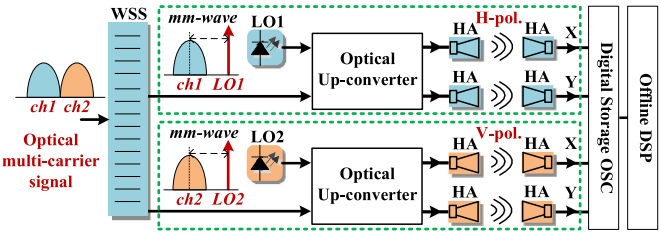

Fig. 13. The schematic diagram of the photonics-aided mm-wave system based on the integration of T-I, T-II, and T-III. WSS: wavelength selective switch.

we use a two-channel WDM signal as an example. At the optical heterodyne up-converter, we first use a wavelength selective switch (WSS) to separate Channel 1 and Channel 2. After optical heterodyne up-conversion, both Channel 1 and Channel 2 are carried by the same mm-wave carrier frequency. Then, we use two pairs of antennas at horizontal-polarization (H-polarization) to deliver Channel 1, and we use another two pairs of antennas at vertical-polarization (V-polarization) to deliver Channel 2. We define this kind of antenna arrangement as antenna polarization multiplexing. The employment of antenna polarization multiplexing can further double the wireless transmission capacity, but requiring doubled optical and electrical devices [19], [26]. Also, we have measured that, for a typical horn antenna (HA), the H- and V-polarization can have >33-dB polarization isolation [19]. Therefore, the employment of antenna polarization multiplexing can effectively suppress the wireless crosstalk between Channel 1 and Channel 2.

Fig. 14 summarizes our 100 Gb/s- and 200 Gb/s-class experimental demonstrations based on the integration of T-I, T-II, and T-III. Particularly, we have realized the simultaneous transmission of 216-Gb/s W-band signal over 0.7-m wireless distance and 224-Gb/s Q-band signal over 1.5-m wireless distance, which forms a >400-Gb/s wireless mm-wave signal transmission at the hybrid Q- and W-band [26].

F. Multiple Mm-Wave Frequency Multiplexing

We then further introduce the fourth technique of the multiple mm-wave frequency multiplexing, denoted by T-IV, into our mm-wave systems to increase the wireless transmission capacity. For this technique, the employed multiple mm-wave carrier frequencies can be located within the same mm-wave band, and also can be located within several different mm-wave bands, just as shown in Fig. 15.

Fig. 16 summarizes our 400 Gb/s- and 1Tb/s-class experimental demonstrations simply based on T-I or based on the

Wireless capacity	Wireless distance	Mm-wave band	Carrier frequency	Modulation format	BER threshold	Applied techniques and Refs.
112Gb/s	2m	Q-band	37.5GHz	PDM-QPSK	3.8×10^{-3}	T-I, T-II, T-III [19]
216Gb/s	0.7m	W-band	100GHz	PDM-QPSK	3.8×10^{-3}	T-I, T-II, T-III [26]
224Gb/s	1.5m	Q-band	37.5GHz	PDM-16QAM	3.8×10^{-3}	T-I, T-II, T-III [26]

Fig. 14. Our 100 Gb/s- and 200 Gb/s-class experimental demonstrations based on the integration of T-I, T-II, and T-III. T-I: wireless MIMO with optical polarization multiplexing. T-II: optical multi-carrier modulation. T-III: antenna polarization multiplexing.

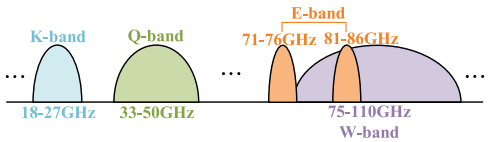

Fig. 15. Schematic diagram of multiple mm-wave frequency multiplexing.

integration of T-I, T-II, T-III, and T-IV. Particularly, we have achieved 1056-Gb/s signal delivery over 3.1-m wireless distance at D-band based on the integration of T-I to T-IV [29], [75]. Our 1056-Gb/s demonstration has employed the high-level 64QAM modulation and the technique of probabilistic constellation shaping (PS), which, as a kind of coded modulation scheme, is one of the recent research hotspots in the field of optical communication [29], [75]–[80]. Here, PS5.5 denotes that the effective bit number per symbol per polarization is 5.5 for the 64QAM signal after PS. Employing the same 64QAM modulation and PS5.5, we have also achieved the single-carrier 352-Gb/s signal delivery over 3.1-m wireless distance at D-band, simply based on T-I [29], [75]. In the following Subsection, we will introduce in detail the principle of the PS and the realization of the 1056-Gb/s wireless transmission capacity.

G. Probabilistic Constellation Shaping (PS)

In this Subsection, the 64QAM modulation is used as an example to explain the principle of the PS. The PS is typically implemented at the transmitter end based on DSP. As shown in Fig. 17(a), each dimension of the two-dimensional 64QAM signal constellation can be considered as an independent 4-ary pulse-amplitude-modulation (PAM-4) signal, the levels of which appear with non-equal probabilities following the Maxwell-Boltzmann distribution [29], [75]–[80].

It is more vivid for us to observe this characteristic of the PS at the receiver end, from the comparison between the recovered normal 64QAM signal constellation and the recovered 64QAM signal constellations after the PS. As shown in Fig. 17(b), for the recovered normal 64QAM signal constellation, each constellation point appears with an equal probability. After the PS, however, the inner constellation points with lower energy appear with larger probabilities, while the outer constellation points with higher energy appear with smaller probabilities. Therefore, the total signal power is reduced after PS.

It is obvious that, however, the employment of the PS will also lead to the reduction of the effective bit number per symbol and therefore the reduction of the effective transmission bit rate. However, the saved energy by the PS is larger than that used to compensate for the loss of the transmission bit rate. Therefore, after the PS, we can still get enough power budget to improve the system performance. Moreover, the employment of the PS can enhance the system tolerance to noise for a certain transmitter power, since the effective Euclidean distance of the 64QAM signal is enhanced after the PS. Also, for a fixed transmission bit rate, the higher the degree of the PS, the higher the transmission baud rate and the higher the requirement for the employed component bandwidth. Since the commercially available components typically have limited bandwidth, a larger transmission baud rate may lead to the filtering effect, which will partially or even completely offset the advantage brought by the PS [79]. As a result, there exists an optimal degree of the PS for a fixed transmission bit rate.

The wireless mm-wave channel is usually power-insufficient because of the lack of high-frequency mm-wave power amplifiers, which will limit the wireless transmission distance or capacity, particularly for the higher-level QAM signals. The introduction of the PS into the wireless mm-wave systems can increase the wireless transmission capacity at a certain transmission distance or extend the wireless transmission distance, without increasing the launch power into the wireless mm-wave channel.

We first experimentally investigated the performance of the PS in a D-band photonics-aided single-carrier mm-wave signal system, and demonstrated that the employment of the 64QAM-PS5.5 can increase the wireless transmission capacity by 1.5 times (i.e., from 240 Gb/s to 352 Gb/s) and the wireless transmission distance by 2 times (i.e., from 1.6 m to 3.1 m) at the same time [29], [75]. Based on the same D-band mm-wave signal system, we further introduced the techniques of the look-up-table (LUT) pre-distortion and Nyquist shaping with a roll-off factor of 0.1 (NQ-0.1), which are both transmitter- and DSP-based, and found a better bit-error-ratio (BER) performance within a larger optical signal-to-noise ratio (OSNR) range can be obtained. We also measured that, enabled by the 64QAM-PS5.5, LUT pre-distortion, and NQ-0.1, the performance of the D-band system is relatively stable when the mm-wave carrier frequency is located within the frequency range from 124 GHz to 152 GHz.

As a result, we selected two D-band carrier frequencies, i.e., 124.5 GHz and 150.5 GHz, from the aforementioned frequency range to realize our 1056-Gb/s demonstration. Our 1056-Gb/s demonstration has employed the 64QAM-PS5.5, LUT pre-distortion, NQ-0.1, as well as the aforementioned T-I to T-IV

Wireless capacity	Wireless distance	Mm-wave band	Carrier frequency	Modulation format	BER threshold	Applied techniques and Refs.
352Gb/s	3.1m	D-band	140GHz	PDM-64QAM-PS5.5	4×10^{-2}	T-I [29, 75]
412Gb/s	0.6m	Q-, V-, W-band	62.5GHz, 97.5GHz, 137.5GHz	PDM-QPSK	2×10^{-2}	T-I, T-II, T-III, T-IV [28]
440Gb/s	1m	Q-, W-band	37.5GHz, 100GHz	PDM-QPSK, PDM-16QAM	3.8×10^{-3}	T-I, T-II, T-III, T-IV [26]
1056Gb/s	3.1m	D-band	124.5, 150.5GHz	PDM-64QAM-PS5.5	4×10^{-2}	T-I, T-II, T-III, T-IV [29, 75]

Fig. 16. Our 400 Gb/s-and 1 Tb/s-class experimental demonstrations based on the integration of T-I, T-II, T-III, and T-IV. T-I: wireless MIMO with optical polarization multiplexing. T-II: optical multi-carrier modulation. T-III: antenna polarization multiplexing. T-IV: multiple mm-wave frequency multiplexing.

[29], [75]. In our 1056-Gb/s demonstration, we have simultaneously delivered two dual-carrier mm-wave signals. Each dual-carrier mm-wave signal has used two mm-wave carriers located at 124.5 GHz and 150.5 GHz, respectively. Each mm-wave carrier carries 24-Gbaud transmitter data, and each 24-Gbaud transmitter data has employed optical polarization multiplexing and 64QAM-PS.5.5. Therefore, 24 Gbaud $\times$ 5.5 $\times$ 2 $\times$ 2 $\times$ 2 yields the total capacity of 1056 Gb/s.

III. Techniques for >100-m Photonics-Aided Long-Distance Mm-Wave Wireless Transmission

Our large-capacity (>100-Gb/s) achievements mentioned in Section II typically have a very short wireless transmission distance of several meters. Therefore it is interesting to further investigate how to increase the wireless transmission distance of photonics-aided mm-wave communication to hundreds of meters, while maintaining its relatively large wireless transmission capacity. Fig. 18 shows various kinds of approaches for the extension of wireless transmission distance for photonics-aided mm-wave communication [81]. The first approach is to employ relatively low-order vector modulation, such as QPSK, 8QAM, and 16QAM. The lower the modulation order, the larger the Euclidean distance and therefore the lower the required receiver sensitivity. A relatively low receiver sensitivity requirement is advantageous to the extension of wireless transmission distance, if the wireless signal transmitting power is fixed. The second approach is to employ large-gain/high-power RF electrical amplifiers (EAs). For example, the commercially available W-band low-noise amplifier (LNA) can have a large gain of ~25 dB within the whole W-band, while the commercially available W-band power amplifier (PA) can have a high output power of over 20 dBm within the frequency range from 77 GHz to 100 GHz. We have experimentally demonstrated that when we add the large-gain LNA and high-power PA into our wireless transmitter/receiver ends, the wireless transmission distance at W-band can be significantly extended [39]. The third approach is to employ heterodyne coherent detection combined with DSP. Compared to homodyne coherent detection, simplified heterodyne coherent detection is much more hardware-efficient

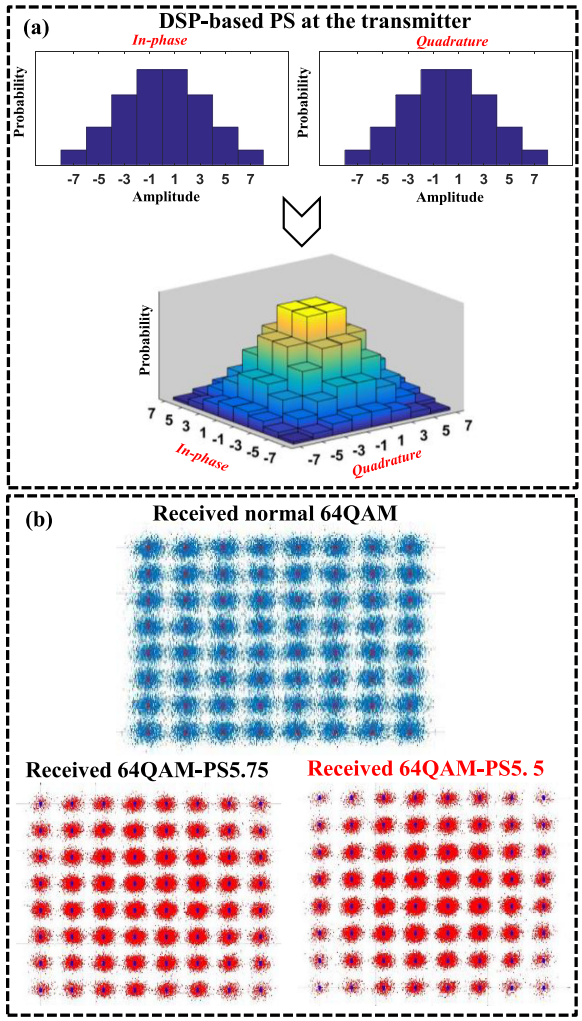

Fig. 17. Principle of the PS from the point of view of the 64QAM signal constellation.

and suitable for system integration [82]. Moreover, the state-of-the-art receiver-based DSP algorithms can effectively improve the receiver sensitivity and system performance [83], [84], and therefore promote the extension of wireless transmission

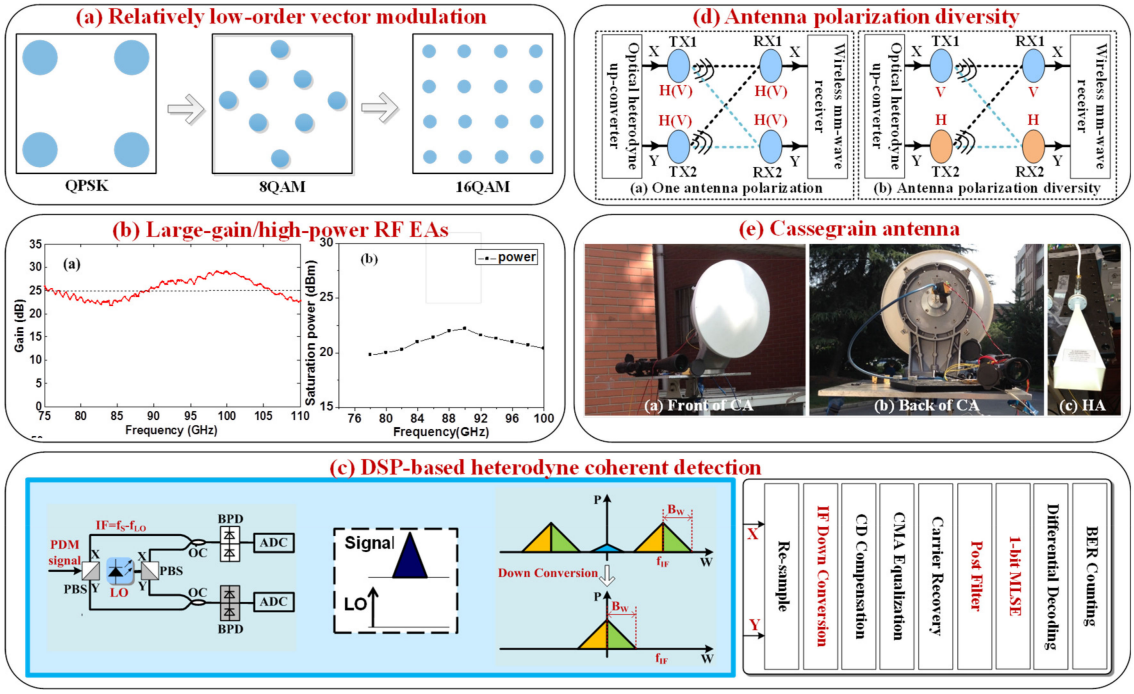

Fig. 18. Various kinds of approaches for the extension of wireless transmission distance for photonics-aided mm-wave communication. (a) Relatively low-order vector modulation. (b) Large-gain/high-power RF EAs. (c) Heterodyne coherent detection combined with DSP. (d) Antenna polarization diversity. (e) The employment of the CA.

Wireless capacity	Wireless distance	Product of capacity and distance	Mm-wave band	Carrier frequency	Modulation format	BER threshold and Refs.
40Gb/s	0.16km	6.4(Gb/s·km)	W-band	85.5GHz	PDM-QPSK	3.8×10^{-3} [38]
100Gb/s	0.1km	10(Gb/s·km)	W-band	96GHz	PDM-QPSK	2×10^{-2} [41]
80Gb/s	0.3km	24(Gb/s·km)	W-band	85.5GHz, 95.5GHz	PDM-QPSK	3.8×10^{-3} [40, 85]
32Gb/s	1km	32(Gb/s·km)	K-band	23GHz	PDM-16QAM	3.8×10^{-3} [42]
20Gb/s	1.7km	34(Gb/s·km)	W-band	85.5GHz	PDM-QPSK	3.8×10^{-3} [39]
32Gb/s	2.5km	80(Gb/s·km)	K-band	23GHz	PDM-16QAM	3.8×10^{-3} [43, 86]
54Gb/s	2.5km	135(Gb/s·km)	W-band	94GHz	PDM-8QAM	3.8×10^{-3} [43, 86]

Fig. 19. Our field-trial demonstrations on >100-m photonics-aided long-distance wireless mm-wave signal transmission.

distance. The fourth approach is to employ antenna polarization diversity. Wireless crosstalk may occur in antenna MIMO, and can become more severe with the increase of wireless transmission distance, which makes the proper adjustment of receiver antennas difficult for long-distance wireless mm-wave transmission. The antenna MIMO based on antenna polarization diversity, in which one pair of antennas is horizontally polarized while the other pair is vertically polarized, can effectively suppress wireless crosstalk and offers an easy antenna installation and adjustment [69]. Therefore, the employment of antenna polarization diversity can effectively promote the extension of wireless transmission distance. The last but not the least approach is to employ the cassegrain antennas (CAs). Compared to the typical HA, the CA has a large gain and a small half-power beamwidth at the cost of a large size and a heavy weight. Therefore, the wireless transmission distance can be extended from several meters with HAs to several kilometers with CAs.

Fig. 19 summarized our field-trial demonstrations on >100-m photonics-aided long-distance wireless mm-wave signal transmission based on the aforementioned five kinds of techniques. Particularly, we have achieved the bidirectional delivery of W-band signal and K-band signal over 2.5-km wireless distance [43], [86]. For W-band downlink, we have used 94-GHz mm-wave carrier, which carries 9-Gbaud (54-Gb/s) PDM-8QAM signal. For K-band uplink, we have used 23-GHz RF carrier,

which carries 4-Gbaud (32-Gb/s) PDM-16QAM signal. For both W-band downlink and K-band uplink, we have employed at each wireless transmitter end two cascaded mm-wave EAs, i.e., a large-gain low-noise amplifier (LNA) cascaded with a high-power power amplifier (PA), which can significantly extend the wireless transmission distance. Our 2.5-km LOS wireless transmission link has been set in the mid-air on a sunny day, while two high buildings are used to locate the wireless transmitter and receiver ends, respectively. A telescope is used at both the wireless transmitter and receiver ends to do the antenna alignment.

In addition, we also proposed the photonic mm-wave demodulation technique, which can implement the electrical-to-optical conversion for the dual-polarization high-speed electrical vector mm-wave signals, so that another fiber-optic transmission is realized after wireless transmission [87]. Based on our aforementioned photonics-aided mm-wave technologies as well as the photonic mm-wave demodulation technique, we also further proposed and experimentally demonstrated several large-capacity bidirectional full-duplex photonic-wireless-photonic systems [88]. As a result, our proposed large-capacity/long-distance photonics-aided mm-wave transmission systems can be potentially applied to the fixed wireless system for the wireless front-haul/back-haul in 5G.

IV. Conclusion

Enabled by photonics-aided mm-wave generation technique, multiple multi-dimensional multiplexing techniques, and state-of-the-art devices, we have achieved the record-breaking wireless transmission capacity up to 1 Tb/s as well as the record-breaking product of wireless transmission capacity and distance up to 54 Gb/s $\times$ 2.5 km. Our investigation and achievements will form the basis for the development, standardization and final implementation of photonics-aided mm-wave communication systems to meet the eMBB challenges in 5G.

References

[1] M. J. Fice *et al.*, "146-GHz millimeter-wave radio-over-fiber photonic wireless transmission system," *Opt. Express*, vol. 20, no. 2, pp. 1769–1774, 2012.

[2] R. Puerta, J. Yu, X. Li, Y. Xu, J. J. Vegas Olmos, and I. Tafur Monroy, "Single-carrier dual-polarization 328-Gb/s wireless transmission in a D-band millimeter wave 2 $\times$ 2 MU-MIMO radio-over-fiber system," *J. Lightw. Technol.*, vol. 36, no. 2, pp. 587–593, Jan. 2018.

[3] Z. Cao, L. Shen, Y. Jiao, X. Zhao, and T. Koonen, "200 Gbps OOK transmission over an indoor optical wireless link enabled by an integrated cascaded aperture optical receiver," in *Proc. Opt. Fiber Commun. Conf.*, San Diego, CA, USA, 2017, Paper Th5A. 6.

[4] P. T. Dat, A. Kanno, T. Umezawa, N. Yamamoto, and T. Kawanishi, "Millimeter- and terahertz-wave radio-over-fiber for 5G and beyond," in *Proc. EEE Photon. Soc. Summer Top. Meeting Series*, San Juan, PR, USA, 2017, pp. 165–166.

[5] A. Nirmalathas *et al.*, "Multi-gigabit indoor optical wireless networks-Feasibility and challenges," in *Proc. EEE Photon. Soc. Summer Top. Meeting Series*, San Juan, PR, USA, 2016, pp. 130–131.

[6] J. Yu, X. Li, and N. Chi, "Faster than fiber: Over 100-Gb/s signal delivery in fiber wireless integration system," *Opt. Express*, vol. 21, no. 19, pp. 22885–22904, 2013.

[7] J. Yu, "Photonics-assisted millimeter-wave wireless communication," *IEEE J. Quantum Electron.*, vol. 53, no. 6, Dec. 2017, Art. no. 8000517.

[8] X. Li, J. Yu, and G.-K. Chang, "Photonics-assisted technologies for extreme broadband 5G wireless communications," *J. Lightw. Technol.*, vol. 37, no. 12, pp. 2851–2865, Jun. 2019.

[9] J. Yu, X. Li, and W. Zhou, "Tutorial: Broadband fiber-wireless integration for 5G+ communication," *APL Photon.*, vol. 3, no. 11, pp. 111101, Jun. 2018.

[10] S. Savory, "Digital filters for coherent optical receivers," *Opt. Express*, vol. 16, no. 2, pp. 804–817, 2008.

[11] P. Winzer, "High-spectral-efficiency optical modulation formats," *J. Lightw. Technol.*, vol. 30, no. 24, pp. 3824–3835, Dec. 2012.

[12] J. Zhang, X. Li, and Z. Dong, "Digital nonlinear compensation based on the modified logarithmic step size," *J. Lightw. Technol.*, vol. 31, no. 22, pp. 3546–3555, Nov. 2013.

[13] E. Ip and J. M. Kahn, "Feedforward carrier recovery for coherent optical communications," *J. Lightw. Technol.*, vol. 25, no. 9, pp. 2675–2692, Sep. 2007.

[14] X. Zhou and J. Yu, "Multi-level, multi-dimensional coding for high-speed and high-spectral-efficiency optical transmission," *J. Lightw. Technol.*, vol. 27, no. 16, pp. 3641–3653, Aug. 2009.

[15] J. Yu and J. Zhang, "Recent progress on high-speed optical transmission," *Digit. Commun. Netw.*, vol. 2, no. 2, pp. 65–76, 2016.

[16] X. Li, Z. Dong, J. Yu, N. Chi, Y. Shao, and G. K. Chang, "Demonstration of ultra-high bit rate fiber wireless transmission system of 108-Gb/s data over 80-km fiber and 2 $\times$ 2 MIMO wireless links at 100 GHz W-band frequency," in *Proc. Opt. Fiber Commun. Conf.*, Anaheim, CA, USA, 2013, Paper JW2A.75.

[17] Z. Dong, J. Yu, X. Li, G. K. Chang, and Z. Cao, "Integration of 112-Gb/s PDM-16QAM wireline and wireless data delivery in millimeter wave RoF system," in *Proc. Opt. Fiber Commun. Conf.*, Anaheim, CA, USA, 2013, Paper OM3D.2.

[18] J. Zhang, J. Yu, N. Chi, Z. Dong, X. Li, and G. K. Chang, "Multichannel 120-Gb/s data transmission over 2 $\times$ 2 MIMO fiber-wireless link at W-band," *IEEE Photon. Technol. Lett.*, vol. 25, no. 8, pp. 780–783, Apr. 2013.

[19] X. Li, J. Yu, J. Zhang, Z. Dong, and N. Chi, "Doubling transmission capacity in optical wireless system by antenna horizontal-and vertical-polarization multiplexing," *Opt. Lett.*, vol. 38, no. 12, pp. 2125–2127, 2013.

[20] X. Li, J. Yu, J. Zhang, F. Li, and J. Xiao, "Antenna polarization diversity for 146 Gb/s polarization multiplexing QPSK wireless signal delivery at W-band," in *Proc. Opt. Fiber Commun. Conf.*, San Francisco, CA, USA, 2014, Paper M3D.7.

[21] X. Li, J. Yu, Z. Cao, J. Zhang, F. Li, and G. K. Chang, "Ultra-high-speed fiber-wireless-fiber link for emergency communication system," in *Proc. Opt. Fiber Commun. Conf.*, San Francisco, CA, USA, 2014, Paper M3D.6.

[22] X. Li, J. Yu, J. Xiao, and Y. Xu, "Fiber-wireless-fiber link for 128-Gb/s PDM-16QAM signal transmission at W-band," *IEEE Photon. Technol. Lett.*, vol. 26, no. 19, pp. 1948–1951, Oct. 2014.

[23] X. Li and J. Yu, "Over 100 Gb/s ultrabroadband MIMO wireless signal delivery system at the D-Band," *IEEE Photon. J.*, vol. 8, no. 5, Oct. 2016, Art. no. 7906210.

[24] X. Li and J. Yu, "Generation and heterodyne detection of >100-Gb/s Q -band PDM-64QAM mm-wave signal," *IEEE Photon. Technol. Lett.*, vol. 29, no. 1, pp. 27–30, Jan. 2017.

[25] X. Li, Y. Xu, and J. Yu, "Over 100-Gb/s V-band single-carrier PDM-64QAM fiber-wireless-integration system," *IEEE Photon. J.*, vol. 8, no. 5, Oct. 2016, Art. no. 7906907.

[26] X. Li, J. Yu, J. Zhang, Z. Dong, F. Li, and N. Chi, "A 400G optical wireless integration delivery system," *Opt. Express*, vol. 21, no. 16, pp. 18812–18819, 2013.

[27] J. Yu, X. Li, J. Zhang, and J. Xiao, "432-Gb/s PDM-16QAM signal wireless delivery at W-band using optical and antenna polarization multiplexing," in *Proc. Eur. Conf. Opt. Commun.*, Cannes, France, 2013, Paper We.3.6.6.

[28] X. Li, J. Yu, J. Xiao, Y. Xu, and L. Chen, "Photonics-aided over 100-Gbaud all-band (D-, W- and V-band) wireless delivery," in *Proc. Eur. Conf. Opt. Commun.*, Düsseldorf, Germany, 2013, pp. 303–305.

[29] X. Li, J. Yu, L. Zhao, K. Wang, W. Zhou, and J. Xiao, "1-Tb/s photonics-aided vector millimeter-wave signal wireless delivery at D-band," in *Proc. Opt. Fiber Commun. Conf.*, San Diego, CA, USA, 2018, Paper Th4D.1.

[30] J. G. Andrews *et al.*, "What will 5G be?," *IEEE J. Sel. Areas Commun.*, vol. 32, no. 6, pp. 1065–1082, Jun. 2014.

[31] E. Gustafsson and A. Jonsson, "Always best connected," *IEEE Wireless Commun.*, vol. 10, no. 1, pp. 49–55, Feb. 2003.

[32] F. Lu, L. Cheng, M. Xu, J. Wang, S. Shen, and G. K. Chang, "Orthogonal and sparse chirp division multiplexing for MMW fiber-wireless integrated systems," *IEEE Photon. Technol. Lett.*, vol. 29, no. 16, pp. 1316–1319, Aug. 2017.

[33] G. Liu *et al.*, "3-D-MIMO with massive antennas paves the way to 5G enhanced mobile broadband: From system design to field trials," *IEEE J. Sel. Areas Commun.*, vol. 35, no. 6, pp. 1222–1233, Jun. 2017.

[34] T. S. Rappaport *et al.*, "Millimeter wave mobile communications for 5G cellular: It will work!," *IEEE Access*, vol. 1, pp. 335–349, 2013.

[35] M. Xu *et al.*, "Bidirectional fiber-wireless access technology for 5G mobile spectral aggregation and cell densification," *J. Opt. Commun. Netw.*, vol. 8, no. 12, pp. B104–B110, 2016.

[36] F. Lu, M. Xu, L. Cheng, J. Wang, J. Zhang, and G.-K. Chang, "Non-orthogonal multiple access with successive interference cancellation in millimeter-wave radio-over-fiber systems," *J. Lightw. Technol.*, vol. 34, no. 17, pp. 4179–4186, Sep. 2016.

[37] M. Xu *et al.*, "Orthogonal multiband CAP modulation based on offset-QAM and advanced filter design in spectral efficient MMW RoF systems," *J. Lightw. Technol.*, vol. 35, no. 4, pp. 997–1005, Feb. 2017.

[38] J. Xiao, X. Li, J. Yu, Y. Xu, Z. Zhang, and L. Chen, "40-Gb/s PDM-QPSK signal transmission over 160-m wireless distance at W-band," *Opt. Lett.*, vol. 40, no. 6, pp. 998–1001, 2015.

[39] J. Xiao, J. Yu, X. Li, Y. Xu, and Z. Zhang, "20-Gb/s PDM-QPSK signal delivery over 1.7-km wireless distance at w-band," in *Proc. Opt. Fiber Commun. Conf.*, Los Angeles, CA, USA, 2015, Paper W4G.4.

[40] X. Li, J. Yu, J. Xiao, Z. Zhang, Y. Xu, and L. Chen, "Field trial of 80-Gb/s PDM-QPSK signal delivery over 300-m wireless distance with MIMO and antenna polarization multiplexing at W-band," in *Proc. Opt. Fiber Commun. Conf.*, Los Angeles, CA, USA, 2015, Paper Th5A.5.

[41] X. Li, J. Yu, and J. Xiao, "100^3 (100 Gb/s $\times$ 100m $\times$ 100 GHz) optical wireless system," in *Proc. Eur. Conf. Opt. Commun.*, Valencia, Spain, Art. no. 0638.

[42] X. Li and J. Yu, "Photonics-aided 32-Gb/s wireless signal transmission over 1 km at K-band," *IEEE Photon. Technol. Lett.*, vol. 29, no. 13, pp. 1120–1123, Jul. 2017.

[43] X. Li *et al.*, "Bidirectional delivery of 54-Gbps 8QAM W-band signal and 32-Gbps 16QAM K-band signal over 20-km SMF-28 and 2500-m wireless distance," in *Proc. Opt. Fiber Commun. Conf.*, Los Angeles, CA, USA, 2017, Paper Th5A.7.

[44] X. Pang *et al.*, "100 Gbit/s hybrid optical fiber-wireless link in the W-band (75–110 GHz)," *Opt. Express*, vol. 19, pp. 24944–24949, 2011.

[45] A. Hirata *et al.*, "120-GHz-band wireless link technologies for outdoor 10-Gbit/s data transmission," *IEEE Trans. Microw. Theory Techn.*, vol. 60, no. 3, pp. 881–895, Mar. 2012.

[46] B. Razavi, "Design of millimeter-wave CMOS radios: A tutorial," *IEEE Trans. Circuits Syst. I, Reg. Papers*, vol. 56, no. 1, pp. 4–16, Jan. 2009.

[47] B. Heydari *et al.*, "Millimeter-wave devices and circuit blocks up to 104 GHz in 90 nm CMOS," *IEEE J. Solid State Circuits*, vol. 42, no. 12, pp. 2893–2903, Dec. 2007.

[48] K. Okada, "Challenges toward millimeter-wave CMOS circuits enhanced by design techniques," in *Proc. 2013 IEEE Int. Elect. Devices Meeting*, 2013, pp. 17–5.

[49] K. K. Tokgoz *et al.*, "A 120 Gb/s 16QAM CMOS millimeter-wave wireless transceiver," in *Proc. IEEE Int. Solid State Circuits Conf.*, 2018, pp. 168–170.

[50] T. Chi *et al.*, "A 64 GHz full-duplex transceiver front-end with an on-chip multifeed self-interference-canceling antenna and an all-passive canceler supporting 4 Gb/s modulation in one antenna footprint," in *Proc. IEEE Int. Solid State Circuits Conf.*, 2018, pp. 76–78.

[51] D. del Rio *et al.*, "Multi-Gbps tri-band 28/38/60-GHz CMOS transmitter for millimeter-wave radio system-on-chip," in *Proc. IEEE MTT-S Int. Microw. Symp.*, 2019, pp. 488–491.

[52] G. Serafino *et al.*, "Photonics for mmW signal generation," in *Proc. 19th Int. Radar Symp.*, 2018, pp. 1–8.

[53] C. Lim, Y. Tian, C. Ranaweera, T. A. Nirmalathas, E. Wong, and K. Lee, "Evolution of radio-over-fiber technology," *J. Lightw. Technol.*, vol. 37, no. 6, pp. 1647–1656, Mar. 2018.

[54] T. Kawanishi, "THz and photonic seamless communications," *J. Lightw. Technol.*, vol. 37, no. 7, pp. 1671–1679, Apr. 2019.

[55] S. E. Alavi *et al.*, "Towards 5G: A photonic based millimeter wave signal generation for applying in 5G access fronthaul," *Sci. Rep.*, vol. 6, 2016, Art. no. 19891.

[56] M. Chen, X. Xiao, J. Yu, X. Li, and F. Li, "Real-time generation and reception of OFDM signals for X -band RoF uplink with heterodyne detection," *IEEE Photon. Technol. Lett.*, vol. 29, no. 1, pp. 51–54, Jan. 2017.

[57] C.-H. Li, M.-F. Wu, C.-H. Lin, and C.-T. Lin, "W-band OFDM RoF system with simple envelope detector down-conversion," in *Proc. Opt. Fiber Commun. Conf.*, Los Angeles, California, 2015, Paper W4G. 6.

[58] S. Mikroulis, M. P. Thakur, and J. E. Mitchell, "Investigation of a robust remote heterodyne envelope detector scheme for cost-efficient E-PON / 60 GHz wireless integration," in *Proc. 16th Int. Conf. Transp. Opt. Netw.*, Graz, Austria, 2014, pp. 1–4.

[59] D. Zibar *et al.*, "High-capacity wireless signal generation and demodulation in 75- to 110-GHz band employing all-optical OFDM," *IEEE Photon. Technol. Lett.*, vol. 23, no. 12, pp. 810–812, Jun. 2011.

[60] T. P. McKenna, A. N. Jeffrey, and R. C. Thomas, "Experimental demonstration of photonic millimeter-wave system for high capacity point-to-point wireless communications," *J. Lightw. Technol.*, vol. 32, no. 20, pp. 3588–3594, Oct. 2014.

[61] L. Tao *et al.*, "Experimental demonstration of 48-Gb/s PDM-QPSK radio-over-fiber system over 40-GHz mm-wave MIMO wireless transmission," *IEEE Photon. Technol. Lett.*, vol. 24, no. 24, pp. 2276–2279, Dec. 2012.

[62] F. Li, Z. Cao, X. Li, Z. Dong, and L. Chen, "Fiber-wireless transmission system of PDM-MIMO-OFDM at 100 GHz frequency," *J. Lightw. Technol.*, vol. 31, no. 14, pp. 2394–2399, Jul. 2013.

[63] S. Inudo, Y. Yoshida, A. Kanno, P. Tien Dat, T. Kawanishi, and K.-I. Kitayama, "On the MIMO channel rank deficiency in W-band MIMO RoF transmissions," in *Proc. Opt. Fiber Commun. Conf.*, Los Angeles, CA, USA, 2015, Paper W4G. 5.

[64] A. Kanno *et al.*, "Optical and millimeter-wave radio seamless MIMO transmission based on a radio over fiber technology," *Opt. Express*, vol. 20, no. 28, pp. 29395–29403, 2012.

[65] C. H. Lin *et al.*, "60-GHz optical/wireless MIMO system integrated with optical subcarrier multiplexing and 2 $\times$ 2 wireless communication," *Opt. Express*, vol. 23, no. 9, pp. 12111–12116, 2015.

[66] M. Morant, J. Prat, and R. Llorente, "Radio-over-fiber optical polarization-multiplexed networks for 3GPP wireless carrier-aggregated MIMO provision," *J. Lightw. Technol.*, vol. 32, no. 20, pp. 3721–3727, Oct. 2014.

[67] X. Li, Z. Dong, J. Yu, N. Chi, Y. Shao, and G. K. Chang, "Fiber-wireless transmission system of 108 Gb/s data over 80 km fiber and 2 $\times$ 2 multiple-input multiple-output wireless links at 100 GHz W-band frequency," *Opt. Lett.*, vol. 37, no. 24, pp. 5106–5108, 2012.

[68] X. Li *et al.*, "Fiber-wireless-fiber link for 100-Gb/s PDM-QPSK signal transmission at W-band," *IEEE Photon. Technol. Lett.*, vol. 26, no. 18, pp. 1825–1828, Sep. 2014.

[69] X. Li, J. Yu, N. Chi, and J. Xiao, "Antenna polarization diversity for high-speed polarization multiplexing wireless signal delivery at W-band," *Opt. Lett.*, vol. 39, no. 5, pp. 1169–1172, 2014.

[70] P. J. Winzer and R.-J. Essiambre, "Advanced modulation formats for high-capacity optical transport networks," *J. Lightw. Technol.*, vol. 24, no. 12, pp. 4711–4728, Dec. 2006.

[71] M. Seimetz, *High-Order Modulation for Optical Fiber Transmission*, vol. 143. Berlin, Germany: Springer, 2009.

[72] P. J. Winzer, "Modulation and multiplexing in optical communications," in *Proc. Conf. Lasers Electro Opt. Conf. Quantum Electron. Laser Sci. Conf.*, 2009, pp. 1–2.

[73] X. Li *et al.*, "120 Gb/s wireless Terahertz-wave signal delivery by 375 GHz-500 GHz multi-carrier in a 2 $\times$ 2 MIMO system," in *Proc. Opt. Fiber Commun. Conf.*, San Diego, CA, USA, 2018, Paper M4J.4.

[74] X. Li *et al.*, "120 Gb/s wireless terahertz-wave signal delivery by 375 GHz-500 GHz multi-carrier in a 2 $\times$ 2 MIMO system," *J. Lightw. Technol.*, vol. 37, no. 2, pp. 606–611, Jan. 2019.

[75] X. Li *et al.*, "1-Tb/s millimeter-wave signal wireless delivery at D-band," *J. Lightw. Technol.*, vol. 37, no. 1, pp. 196–204, Jan. 2019.

[76] C. Pan and F. R. Kschischang, "Probabilistic 16-QAM shaping in WDM systems," *J. Lightw. Technol.*, vol. 34, no. 18, pp. 4285–4292, Sep. 2016.

[77] F. Buchali, F. Steiner, G. Böcherer, L. Schmalen, P. Schulte, and W. Idler, "Rate adaptation and reach increase by probabilistically shaped 64-QAM: An experimental demonstration," *J. Lightw. Technol.*, vol. 34, no. 7, pp. 1599–1609, Apr. 2016.

[78] Y. Zhu *et al.*, "Spectrally-efficient single-carrier 400G transmission enabled by probabilistic shaping," in *Proc. Opt. Fiber Commun. Conf.*, Los Angeles, CA, USA, 2017, Paper M3C.1.

[79] J. Yu *et al.*, "8 $\times$ 506-Gb/s 16QAM WDM signal coherent transmission over 6000-km enabled by PS and HB-CDM," in *Proc. Opt. Fiber Commun. Conf.*, San Diego, CA, USA, 2018, Paper M2C.3.

[80] K. Wang, X. Li, M. Kong, P. Gou, W. Zhou, and J. Yu, "Probabilistically shaped 16QAM signal transmission in a photonics-aided wireless Terahertz-wave system," in *Proc. Opt. Fiber Commun. Conf.*, San Diego, CA, USA, 2018, Paper M4J.7.

[81] X. Li, J. Yu, and G.-K. Chang, "Photonics-aided mm-wave communication for 5G," in *Proc. Opt. Fiber Commun. Conf.*, San Diego, CA, USA, 2019, Paper Th1F.1.

[82] X. Li, J. Xiao, and J. Yu, "Heterodyne detection and transmission of 60-Gbaud PDM-QPSK signal with SE of 4 b/s/Hz," *Opt. Express*, vol. 22, no. 8, pp. 9307–9313, 2014.

[83] J. Yu, Z. Dong, H. Chien, Z. Jia, M. Gunkel, and A. Schippel, "Field trial Nyquist-WDM transmission of 8 × 216.4 Gb/s PDM-CSRZ-QPSK exceeding 4 b/s/Hz spectral efficiency," in *Proc. Opt. Fiber Commun. Conf.*, Los Angeles, CA, 2012, Paper PDP5D.3.

[84] J. Yu and X. Zhou, "Ultra-high-capacity DWDM transmission system for 100G and beyond," *IEEE Commun. Mag.*, vol. 48, no. 3, pp. S56–S64, Mar. 2010.

[85] X. Li, J. Yu, and J. Xiao, "Demonstration of ultra-capacity wireless signal delivery at W-band," *J. Lightw. Technol.*, vol. 34, no. 1, pp. 180–187, Jan. 2016.

[86] X. Li *et al.*, "Delivery of 54-Gbps 8QAM W-band signal and 32-Gbps 16QAM K-band signal over 20-km SMF-28 and 2500-m wireless distance," *J. Lightw. Technol.*, vol. 36, no. 1, pp. 50–56, Jan. 2018.

[87] C. Tang *et al.*, "A 30 Gb/s full-duplex bi-directional transmission optical wireless-over fiber integration system at W-band," *Opt. Express*, vol. 22, no. 1, pp. 239–245, 2014.

[88] Y. Xu, J. Yu, X. Li, J. Xiao, and G. K. Chang, "Demonstration of 120 Gbit/s full-duplex signal transmission over fiber-wireless-fiber network at W-band," in *Proc. Opt. Fiber Commun. Conf.*, Los Angeles, CA, USA, 2015, Paper W4G.7.